

Supporting Information

Tuning the electronic properties of Fe(II)-NHC sensitizers with thienyl π -extended ligands

Nour Shalhoub,^a Edoardo Marchini,^{*b} Federico Coppola,^{c,§} Roberto Argazzi,^d Stefano Caramori,^b Mariachiara Pastore,^{*c} Philippe Pierrat,^a and Philippe C. Gros,^{*a,e}

Contents

Synthesis of complexes	2
General	2
Synthesis of NS158	2
Synthesis of NS271	3
Synthesis of NS252	3
NMR Spectra.....	4
Liquid chromatograms	8
Calculated opto-electronic properties	10
Characterization of FeNHC-sensitized photoanodes	19

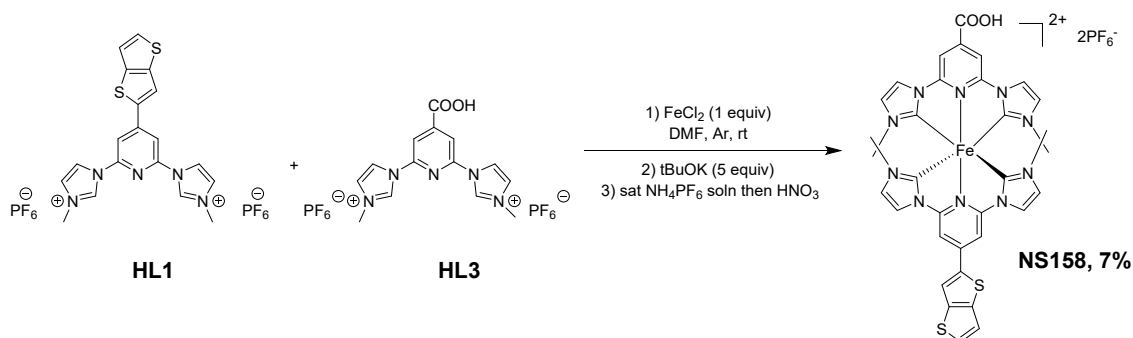
Synthesis of complexes

General

Solvents were purified by standard procedures and purged with argon before use. All other chemicals used in this work were of analytical grade and were used without further purification until or unless stated, and all reactions were performed under an inert atmosphere of argon. Chromatographic separations were carried out on silica gel (60–120 mesh). ^1H (400 MHz) and ^{13}C NMR (100 MHz) spectra were taken on a DRX400 Bruker spectrometer at ambient temperature. High-resolution mass spectrometry (HRMS) data was obtained by using Bruker micrOTOF-Q spectrometer. UV-vis spectra were recorded in a 1 cm path length quartz cell on a LAMBDA 1050 (Perkin Elmer), spectrophotometer.

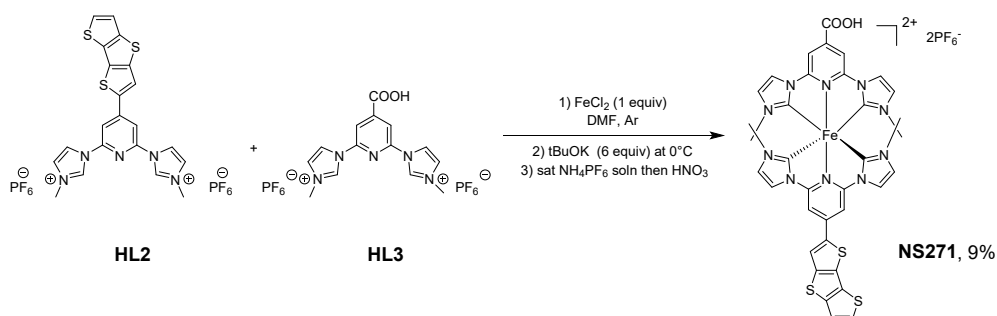
The preligands **HL1**,^[1] **HL2**,^[1] **HL3**^[2] and **HL4**^[2] were prepared following previously reported procedures. **ARM15** was prepared from ref [3]. Liquid chromatography high resolution mass spectrometry (LC–HRMS) analysis of complexes (**NS158**, **NS271** and **NS252**) was performed on a XevoXS G2 Waters instrument. Separation used a 1.9 μm , 20*2.1mm Hypersil gold C18 column (NS158 and NS252) and a 1.8 μm 50*2.1 mm Restek force biphenyl column (NS271). Mobile phase A was water + 0.1% formic acid, mobile phase B was acetonitrile and mobile phase C was methanol. The gradient for the separation on C18 was: 0–0.5 min, 95% A and 5% B; 0.5–12 min, 1% A and 99%B and then continuous 95% A and 5% B. Flow rate was 0.5 mL min⁻¹; injection volume 2 μL . The gradient for the separation on biphenyl column was: 0–0.5 min, 95% A, 5%C; 0.5–4.0 min, 80% A, 20% C; 4.0–11 min, 1%A, 49% B and 50% C and then continuous 95%A, 5%C. Flow rate was 0.8 mL min⁻¹; injection volume 2 μL .

Synthesis of NS158



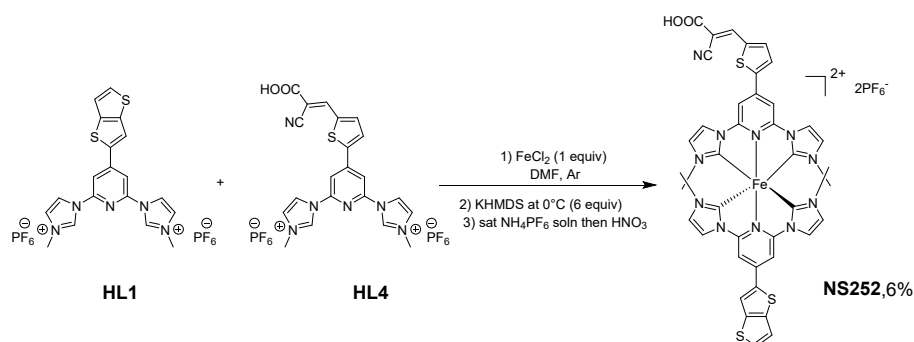
HL1 (95 mg, 0.142 mmol), **HL3** (80 mg, 0.142 mmol) and FeCl_2 (18 mg, 0.142 mmol) were dried under vacuum at 80°C overnight. After 3 cycles of vacuum/argon, anhydrous DMF (2 ml) was added. 3 cycles of freeze-pump-thaw were performed to degas the reaction mixture and t-BuOK was added at once (0.71 mmol, 0.08 g) at room temperature. The color directly changed from yellow to purple upon addition of t-BuOK. After 1 h, the reaction was completed (seen by TLC monitoring). The reaction mixture was filtered over celite and recovered in acetonitrile. After evaporation of acetonitrile, a saturated solution of NH_4PF_6 was added (10 mL), followed by HNO_3 until the solution becomes acidic (pH= 2) and the precipitate was collected by filtration. Then, the crude was purified on silica gel column chromatography using acetone/ $\text{H}_2\text{O}/\text{KNO}_3$ (10/3/0.5). The heteroleptic fraction was collected and after evaporation of acetone, a solution of NH_4PF_6 was added followed by HNO_3 until the solution becomes acidic (pH= 2) affording the precipitation of the desired complex **NS158**. The latter was recovered by filtration, washed with diethyl ether and dried under vacuum. The isolated complex **NS158** was obtained as a pink colored compound (20 mg, 7% yield). ^1H NMR (400 MHz, acetonitrile- d_3) δ 8.34 (s, 2H), 8.26 (s, 1H), 8.19 (d, J = 2.2 Hz, 2H), 8.15 (d, J = 2.2 Hz, 2H), 8.05 (s, 2H), 7.73 (d, J = 5.3 Hz, 1H), 7.49 (d, J = 5.3 Hz, 1H), 7.04 (d, J = 2.1 Hz, 2H), 7.02 (d, J = 2.1 Hz, 2H), 2.64 (s, 6H), 2.51 (s, 6H). ^{13}C { ^1H } NMR (101 MHz, CD_3CN) δ 200.8, 200.6, 155.3, 154.8, 145.5, 142.5, 142.2, 141.4, 132.2, 127.6, 127.5, 121.4, 121.1, 117.7, 117.5, 105.9, 102.4, 35.7, 35.2. ESI-HRMS calcd for $\text{C}_{33}\text{H}_{28}\text{FeN}_{10}\text{O}_2\text{S}_2$ m/z = 358.0588. Found: 358.0595.

Synthesis of NS271



HL2 (79 mg, 0.142 mmol), **HL3** (100 mg, 0.142 mmol), and FeCl_2 (18 mg, 0.142 mmol) were dried under vacuum at 80°C overnight. 3 cycles of vacuum/argon were done and anhydrous DMF (2 mL) was added. Then, 3 cycles of freeze-pump-thaw were performed for solvent degassing. t-BuOK (0.852 mmol, 0.095 g) was added at once at 0°C and the color of the reaction mixture directly changed from yellow to purple upon addition of the base. After 1 h, the reaction was complete and the reaction mixture was filtered over celite and recovered in acetonitrile. After evaporation of acetonitrile, a saturated solution of NH_4PF_6 was added (10 mL), followed by HNO_3 until the solution becomes acidic ($\text{pH} = 2$) and the precipitate was collected by filtration. Then, the crude was purified on silica gel column chromatography using acetone/ $\text{H}_2\text{O}/\text{KNO}_3$ (10/3/0.5). The heteroleptic fraction was collected and after evaporation of acetone, a solution of NH_4PF_6 was added followed by HNO_3 until the solution becomes acidic ($\text{pH} = 2$) affording the precipitation of the desired complex **C2**. The latter was recovered by filtration, washed with diethyl ether and dried under vacuum. The isolated complex **NS271** was obtained as a dark pink colored compound (13 mg, 9% yield). ^1H NMR (400 MHz, acetonitrile- d_3) δ 8.31 (s, 1H), 8.29 (s, 1H), 8.17 (d, $J = 2.2$ Hz, 2H), 8.14 (d, $J = 2.2$ Hz, 2H), 8.05 (s, 2H), 7.69 (d, $J = 5.3$ Hz, 1H), 7.5 (d, $J = 5.3$ Hz, 1H), 7.03 (d, $J = 2.2$ Hz, 2H), 7.02 (d, $J = 2.2$ Hz, 2H), 2.64 (s, 6H), 2.5 (s, 6H). ^{13}C NMR (101 MHz, CD_3CN) δ 200.6, 200.4, 165.7, 155.5, 154.7, 145.2, 144.9, 143.7, 141.0, 138.7, 133.6, 130.2, 127.7, 122.9, 122.3, 117.7, 117.6, 105.6, 102.4, 35.7, 35.6. ESI-HRMS calcd for $\text{C}_{35}\text{H}_{28}\text{FeN}_{10}\text{O}_2\text{S}_3$ $m/z = 386.0449$. Found: 386.0446.

Synthesis of NS252

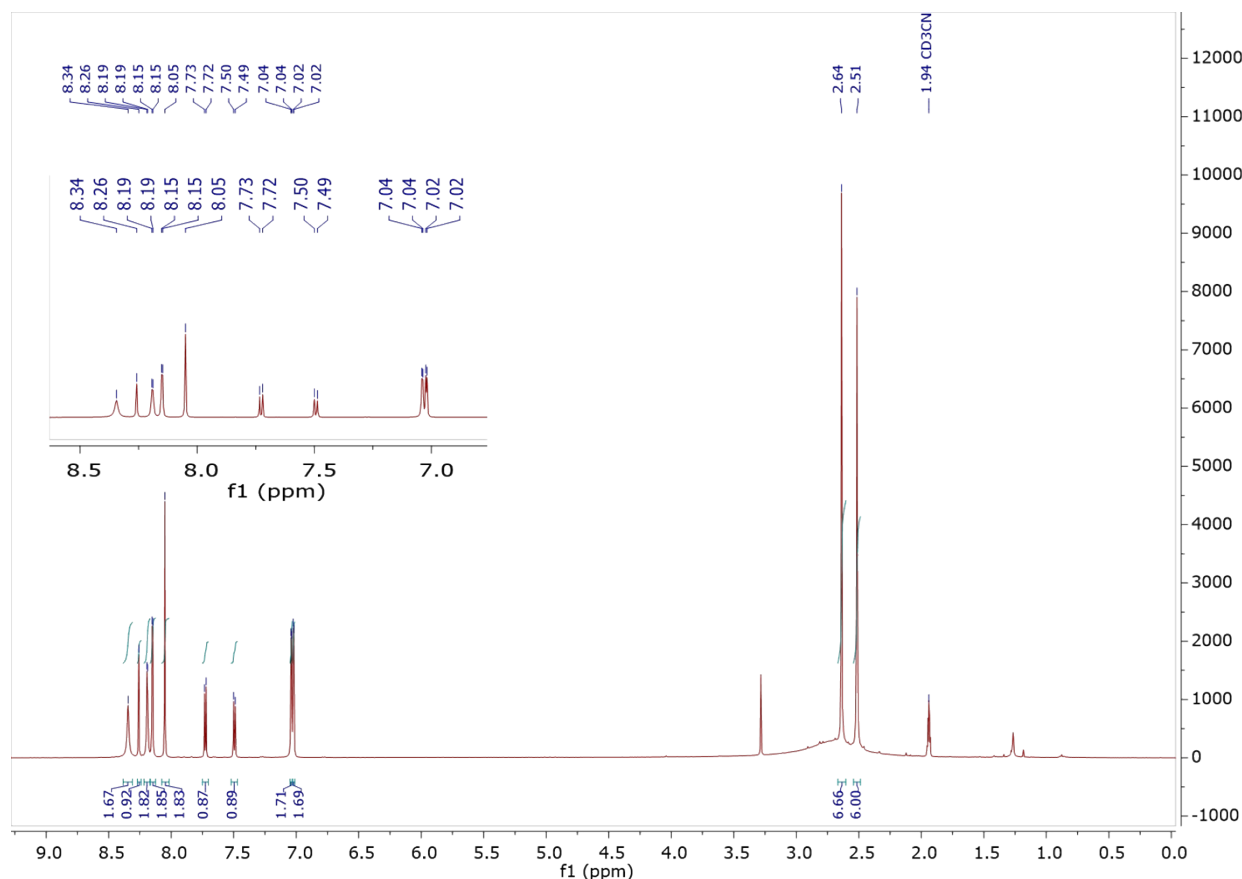


HL1 (95 mg, 0.142 mmol), **HL4** (100 mg, 0.142 mmol), and FeCl_2 (18 mg, 0.142 mmol) were dried under vacuum at 80°C overnight. 3 cycles of vacuum/argon were done and anhydrous DMF (2 mL) was added. Then, 3 cycles of freeze-pump-thaw were performed for solvent degassing. KHMDS (0.85 mmol, 0.85 mL, 1M) was added at 0°C under argon during which the color directly changed from brown to violet. After 2 h, the reaction was completed and the reaction mixture was filtered over celite and recovered in acetonitrile. After evaporation of acetonitrile, a saturated solution of NH_4PF_6 was added

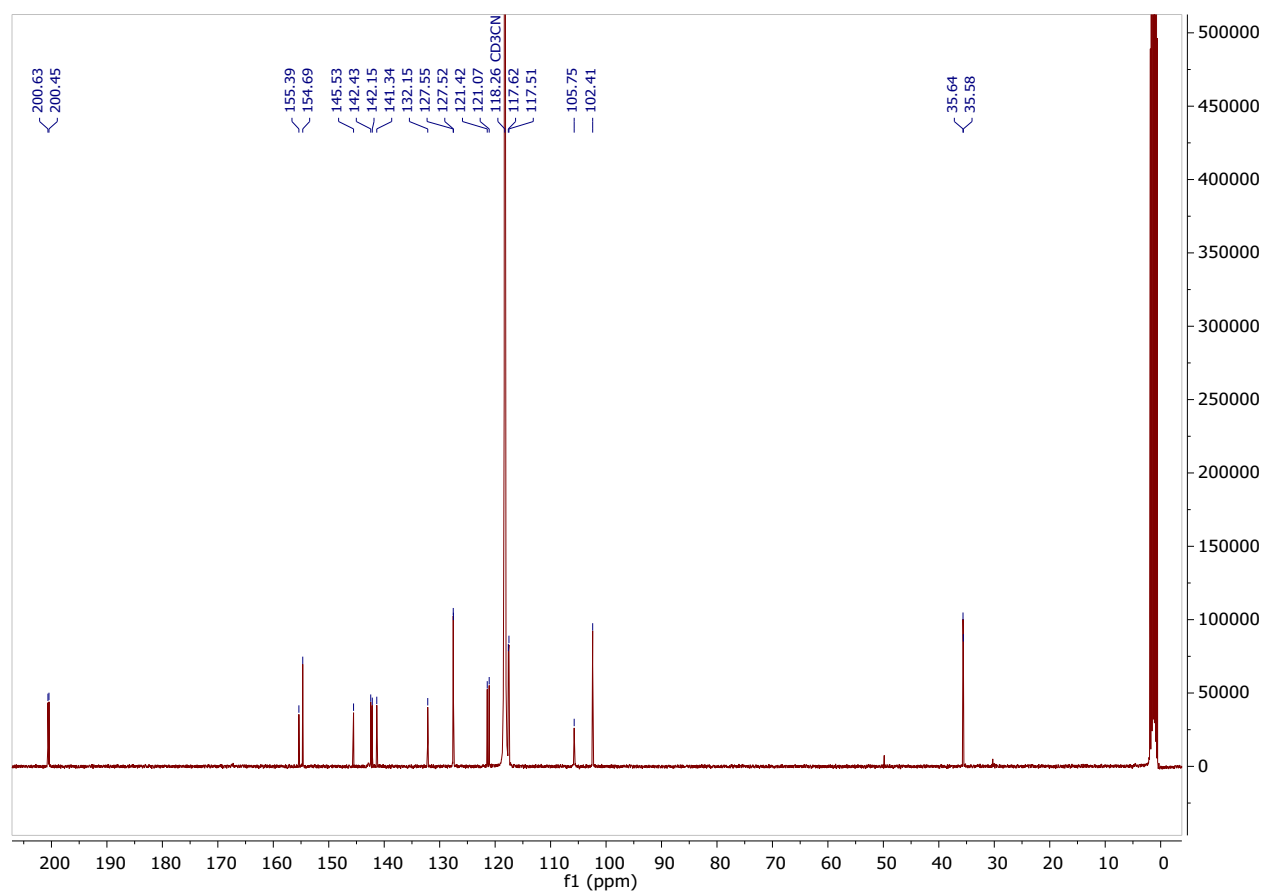
(10 mL), followed by HNO_3 until the solution becomes acidic ($\text{pH} = 2$) and the precipitate was collected by filtration. Then, the crude was purified on silica gel column chromatography using acetone/ $\text{H}_2\text{O}/\text{KNO}_3$ (10/1/0.3). The heteroleptic fraction was collected and after evaporation of acetone, a solution of NH_4PF_6 was added followed by HNO_3 until the solution becomes acidic ($\text{pH} = 2$) affording the precipitation of the desired complex **NS252**. The latter was recovered by filtration, washed with diethyl ether and dried under vacuum. The isolated complex **NS252** was obtained as a violet solid (10 mg, 6% yield). ^1H NMR (400 MHz, Acetonitrile- d_3) δ 8.52 (s, 1H), 8.25 (s, 1H), 8.18 (d, $J = 2.5$ Hz, 2H), 8.15 (d, $J = 2.5$ Hz, 2H), 8.11 (s, 2H), 8.07 (d, $J = 4.1$ Hz, 1H), 8.05 (s, 2H), 7.99 (m, 1H), 7.14 (d, $J = 5$ Hz, 1H), 7.50 (d, $J = 5$ Hz, 1H), 7.04 (m, 4H), 2.63 (s, 6H), 2.58 (s, 6H). ^{13}C NMR (101 MHz, CD_3CN) δ 201.1, 200.9, 155.1, 154.9, 142.6, 142.1, 141.4, 132.2, 132.0, 131.8, 129.2, 127.6, 127.5, 121.3, 121.1, 117.6, 117.5, 102.8, 102.3, 100.4, 99.7, 35.7, 30.9. ESI-HRMS calcd for $\text{C}_{40}\text{H}_{31}\text{FeN}_{11}\text{O}_2\text{S}_3$ $m/z = 424.5582$. Found: 424.5580.

NMR Spectra

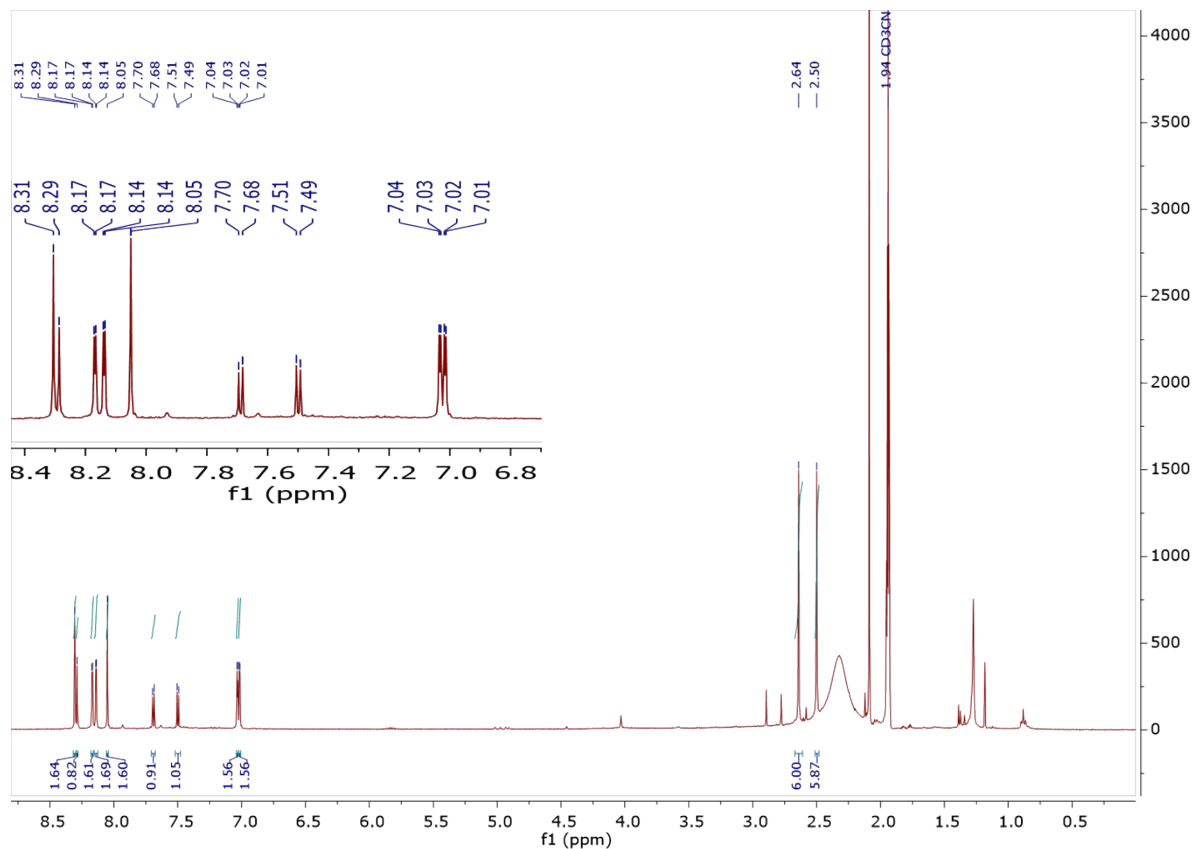
^1H NMR for NS158:



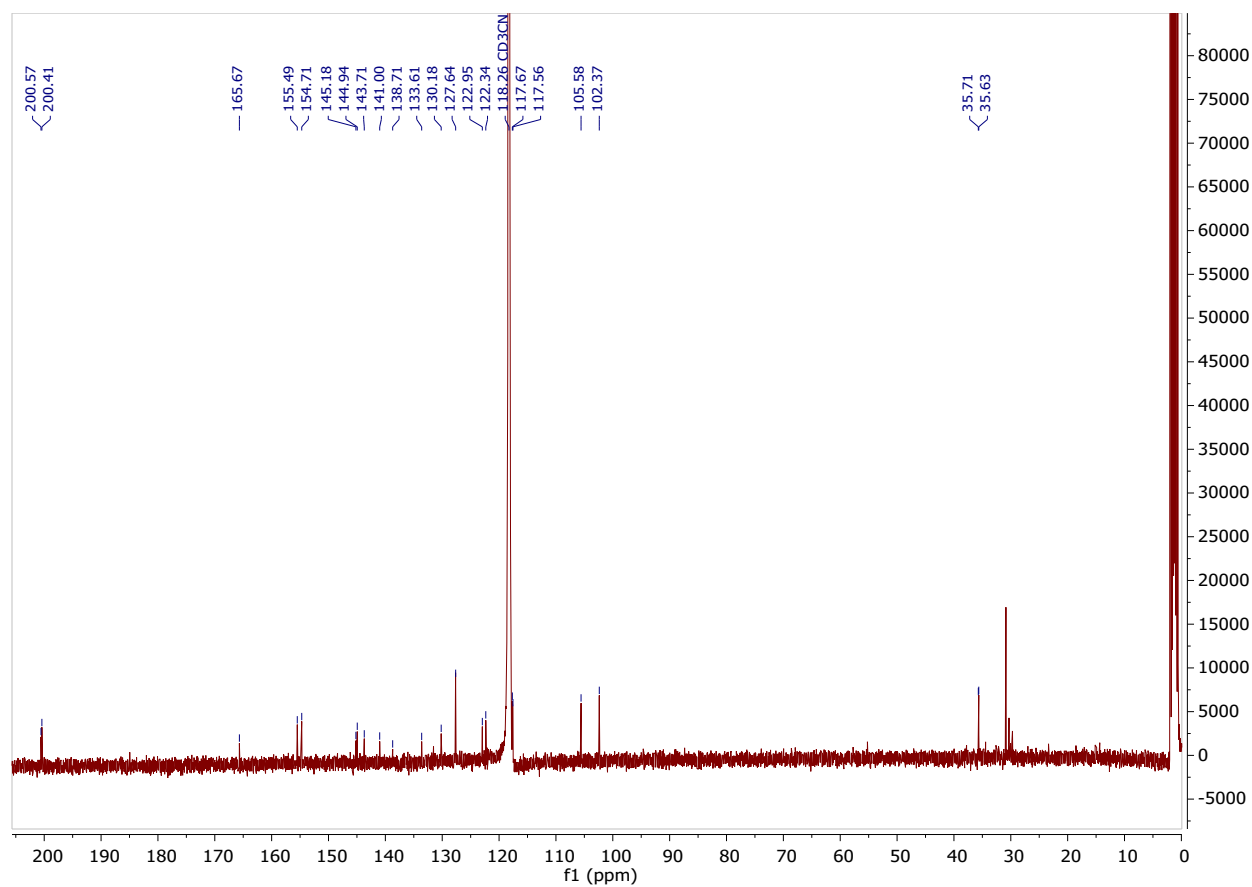
^{13}C NMR for NS158:



^1H NMR for NS271:



¹³C NMR for NS271 :

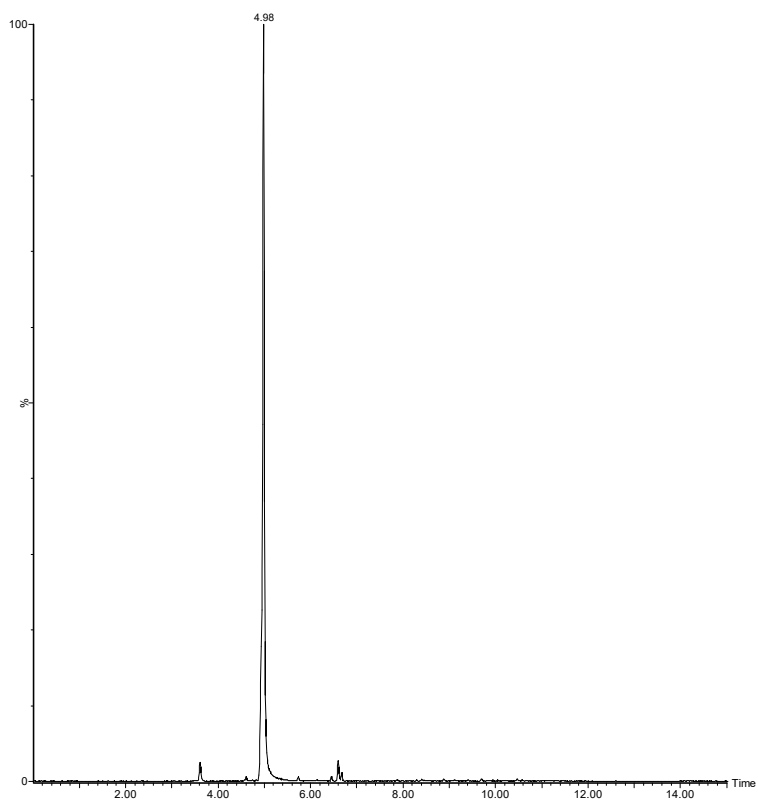


¹H NMR for NS252

Liquid chromatograms

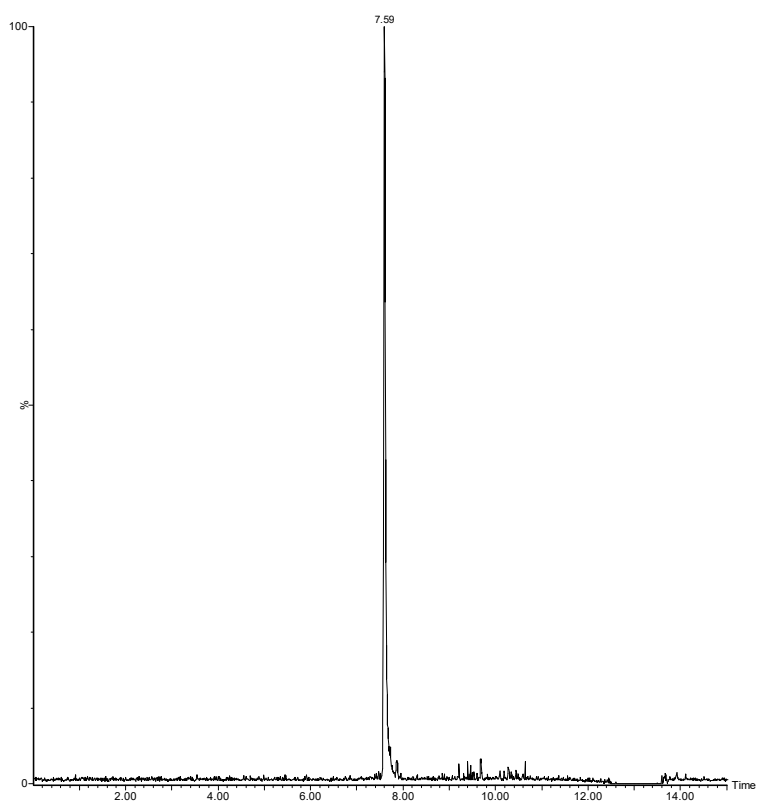
LC for NS158

10 ug/mL MeOH



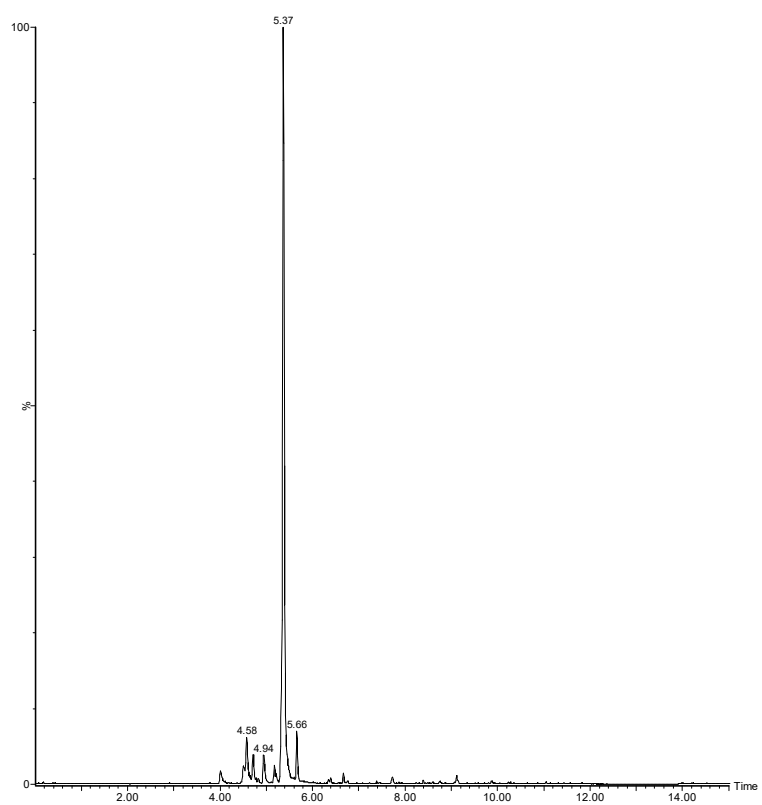
LC for NS271

10ug/mL dans MeOH



LC for NS252

10 ug/mL MeOH



Calculated opto-electronic properties

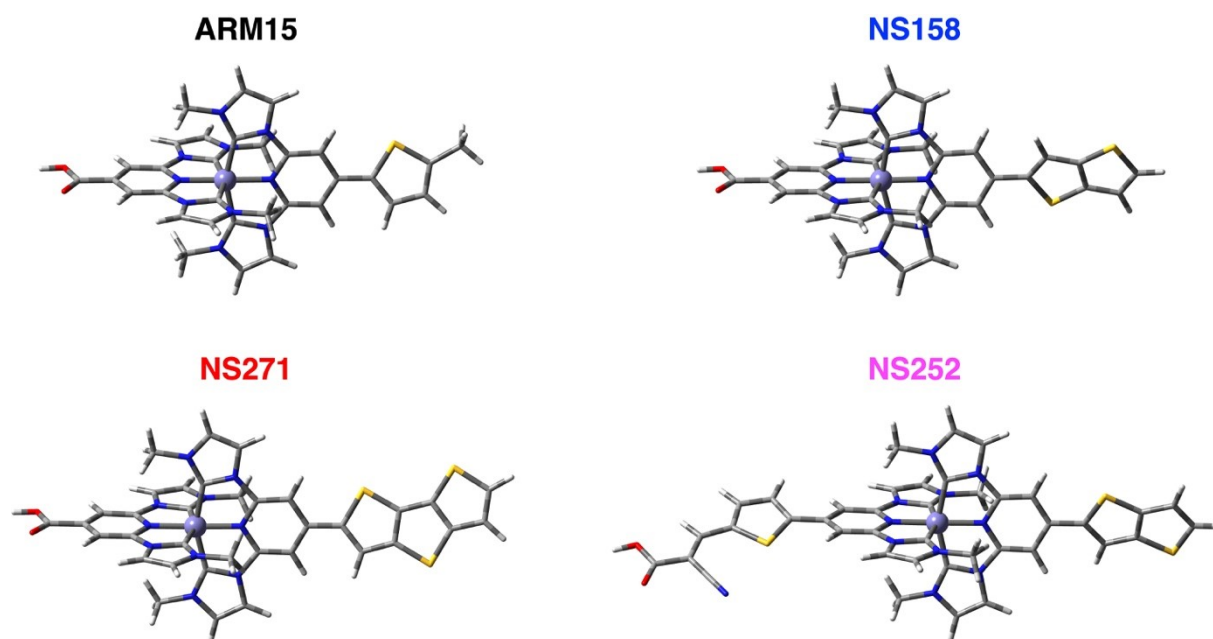


Figure S1: Optimized geometries of **ARM15**, **NS158**, **NS271**, and **NS252** complexes investigated in this work. Each complex features a central Fe(II) ion coordinated by pyridyl–NHC ligands extended with fused thiophene units of variable number. Atom colour code: Fe (purple sphere), N (blue), O (red), S (yellow), C (grey), and H (white).

Table S1: Vertical excitation energies (VEE, in eV), wavelengths (λ , in nm), oscillator strengths (f), and dominant electronic transitions for the bright low-lying singlet excited states of the four investigated dyes (**ARM15**, **NS158**, **NS271**, and **NS252**). The transitions are reported as excitations between molecular orbitals with their corresponding percentage contributions in parentheses.

Dye	Excited State	VEE (eV)	λ (nm)	f	Transition (CI %)
ARM15	4	2.65	468	0.3862	H-2 - L (77.1) H-1 - L+1 (12.0)
	6	2.84	436	0.2144	H-1 - L+1 (66.3) H - L+2 (20.1)
	9	3.19	388	0.2101	H - L+3 (100.0)
NS158	4	2.63	472	0.5522	H-2 - L (70.0) H-1 - L+1 (23.0)
	6	2.79	445	0.2233	H-1 - L+1 (58.8) H - L+2 (21.8)
	10	3.19	389	0.2230	H - L+3 (61.3) H - L+2 (18.0)
NS271	4	2.58	479	0.9723	H-1 - L+1 (48.0) H-2 - L (46.0)
	6	2.73	453	0.1339	H-1 - L+1 (37.0) H-2 - L (32.3) H - L+2 (23.7)
	10	3.12	397	0.4660	H-3 - L+1 (53.2) H - L +2 (37.6)
NS252	3	2.38	521	0.7195	H-2 - L (93.0)
	8	2.90	427	0.5057	H-1 - L+1 (75.8) H - L+3 (11.0)
	13	3.29	377	0.5507	H-5 - L (49.0) H - L+3 (14.0) H-6 - L (13.7)

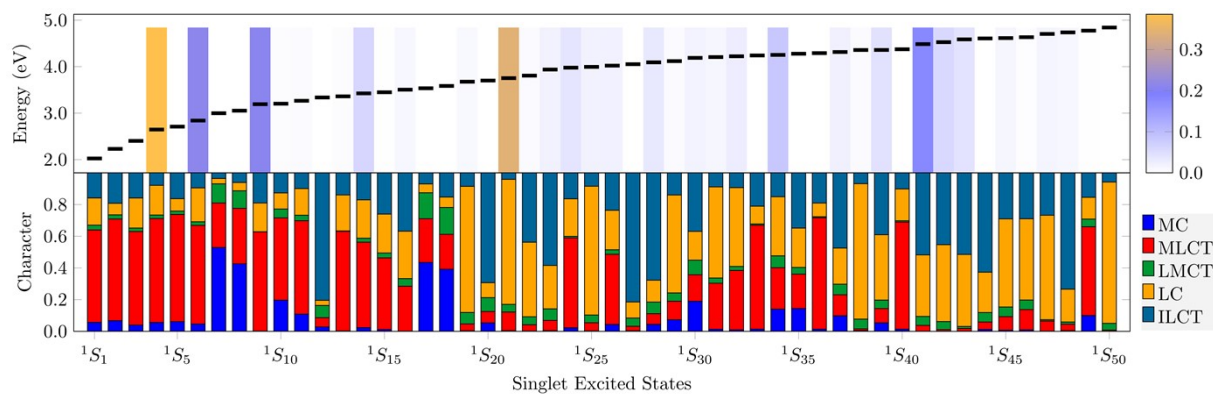


Figure S2: Vertical excitation energies (top panel) and electronic character decomposition (bottom panel) of the first 50 singlet excited states of **ARM15** computed at the Franck–Condon geometry. The color shading represents the oscillator strength (f). The stacked bar plots (bottom panel) report the character of each excited state, decomposed into metal-centered (MC, azure), metal-to-ligand charge transfer (MLCT, red), ligand-to-metal charge transfer (LMCT, green), ligand-centered (LC, orange), and inter-ligand charge transfer (ILCT, blue) contributions.

ARM15	<i>hole</i> ⁺	NTO	<i>electron</i> ⁻	Occ. %
¹S₄		→		78 %
		→		12 %
¹S₆		→		69 %
		→		28 %
¹S₉		→		97 %

Figure S3: Natural transition orbitals (NTOs) corresponding to the lowest-energy bright singlet excitations of **ARM15**, computed at the Franck–Condon geometry. Only the NTO pair with the highest occupation number (Occ., %) is shown for each state. An isovalue of 0.02 a.u. was used for orbital visualization.

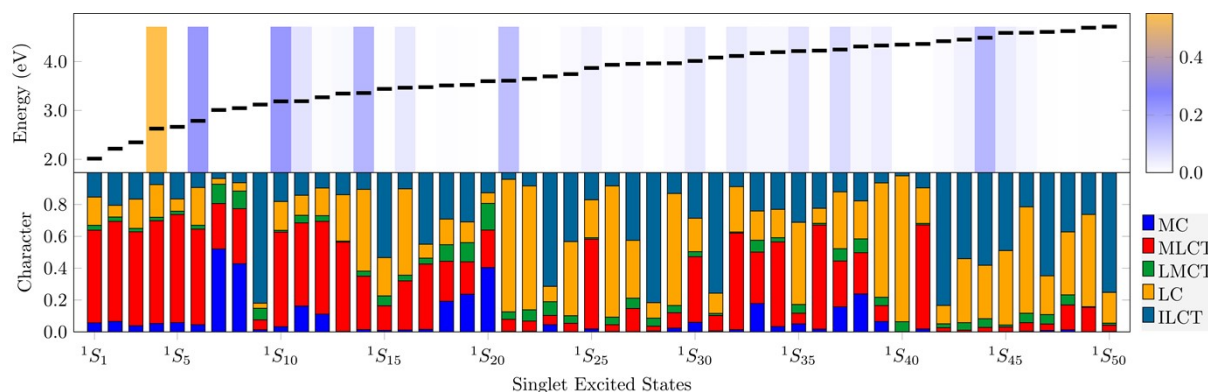


Figure S4: Vertical excitation energies (top panel) and electronic character decomposition (bottom panel) of the first 50 singlet excited states of **NS158** computed at the Franck–Condon geometry. The color shading represents the oscillator strength (f). The stacked bar plots (bottom panel) report the character of each excited state, decomposed into metal-centered (MC, azure), metal-to-ligand charge transfer (MLCT, red), ligand-to-metal charge transfer (LMCT, green), ligand-centered (LC, orange), and inter-ligand charge transfer (ILCT, blue) contributions.

NS158	<i>hole</i> ⁺	NTO	<i>electron</i> ⁻	Occ. %
¹S₄		→		70 %
		→		23 %
¹S₆		→		62 %
		→		28 %
¹S₁₀		→		80 %
		→		11 %

Figure S5: Natural transition orbitals (NTOs) corresponding to the lowest-energy bright singlet excitations of **NS158**, computed at the Franck–Condon geometry. Only the NTO pair with the highest occupation number (Occ., %) is shown for each state. An isovalue of 0.02 a.u. was used for orbital visualization.

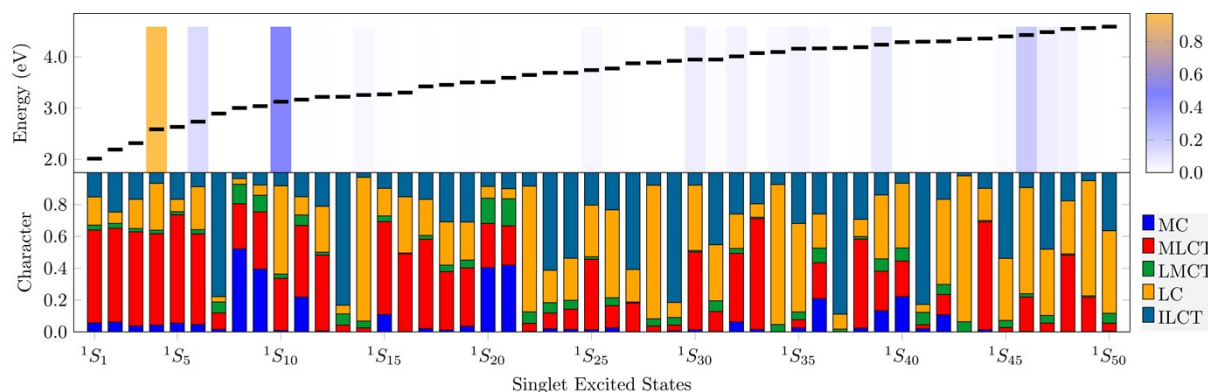


Figure S6: Vertical excitation energies (top panel) and electronic character decomposition (bottom panel) of the first 50 singlet excited states of **NS271** computed at the Franck–Condon geometry. The color shading represents the oscillator strength (f). The stacked bar plots (bottom panel) report the character of each excited state, decomposed into metal-centered (MC, azure), metal-to-ligand charge transfer (MLCT, red), ligand-to-metal charge transfer (LMCT, green), ligand-centered (LC, orange), and inter-ligand charge transfer (ILCT, blue) contributions.

NS271	<i>hole</i> ⁺	NTO	<i>electron</i> ⁻	Occ. %
¹S₄		→		51 %
		→		46 %
¹S₆		→		40 %
		→		32 %
¹S₁₀		→		61 %
		→		38 %

Figure S7: Natural transition orbitals (NTOs) corresponding to the lowest-energy bright singlet excitations of **NS271**, computed at the Franck–Condon geometry. Only the NTO pair with the highest occupation number (Occ., %) is shown for each state. An isovalue of 0.02 a.u. was used for orbital visualization.

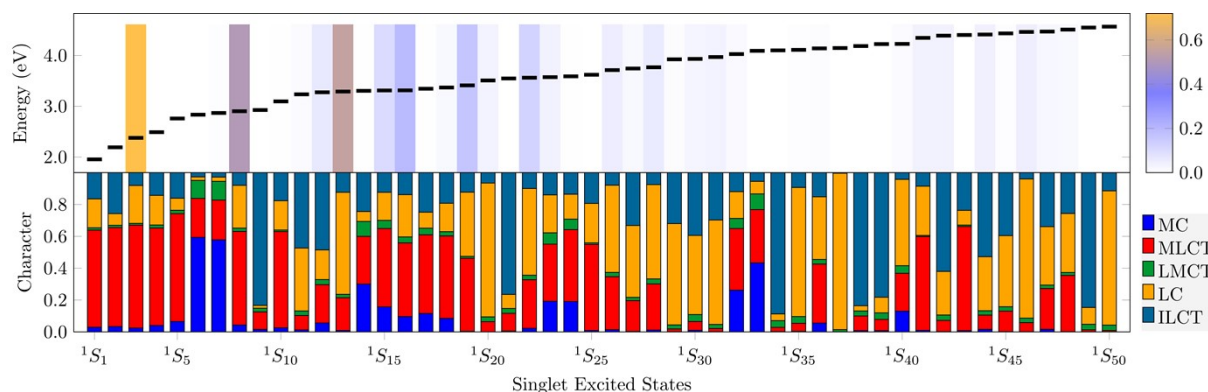


Figure S8: Vertical excitation energies (top panel) and electronic character decomposition (bottom panel) of the first 50 singlet excited states of **NS252** computed at the Franck–Condon geometry. The color shading represents the oscillator strength (f). The stacked bar plots (bottom panel) report the character of each excited state, decomposed into metal-centered (MC, azure), metal-to-ligand charge transfer (MLCT, red), ligand-to-metal charge transfer (LMCT, green), ligand-centered (LC, orange), and inter-ligand charge transfer (ILCT, blue) contributions.

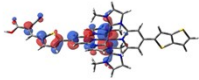

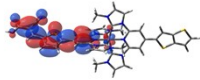
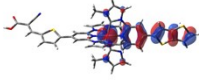
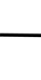
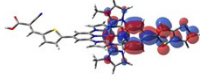
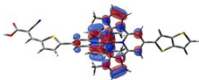

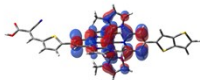
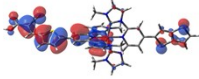
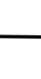
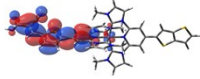
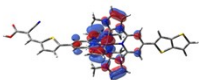
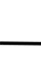
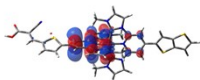
NS252	<i>hole</i> ⁺	NTO	<i>electron</i> ⁻	Occ. %
¹S₃				94 %
¹S₈				80 %
				15 %
¹S₁₃				69 %
				15 %

Figure S9: Natural transition orbitals (NTOs) corresponding to the lowest-energy bright singlet excitations of **NS252**, computed at the Franck–Condon geometry. Only the NTO pair with the highest occupation number (Occ., %) is shown for each state. An isovalue of 0.02 a.u. was used for orbital visualization.

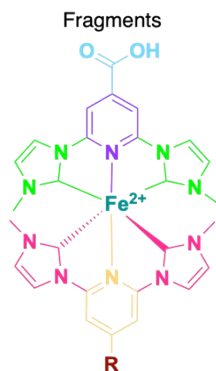


Figure S10: Schematic representation of the Fe(II) complex showing the molecular fragments used for the analysis of *hole* (h^+) – *electron* (e^-) fractions in the investigated dyes. The carboxylic anchoring group is highlighted in light blue, the pyridine and the carbene groups in the anchoring group in violet and light green, respectively; the pyridine and the carbene groups in the substituted ligand in orange and pink, respectively; the central Fe(II) ion in teal, and the R group in bordeaux.

Table S2: Hole (h^+) and electron (e^-) population fractions over the seven fragments for the lowest and bright singlet excited states of the investigate Fe(II) heteroleptic dyes. Population fractions larger than 0.1 are highlighted in bold. Refer to **Fig. S10** for labeling scheme.

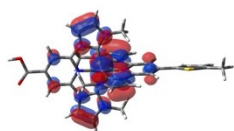
Dye	Excited State	Fragments	h^+	e^-
ARM15	4	Fe	0.71133	0.07815
		C ₈ H ₁₀ N ₄	0.08124	0.08950
		C ₅ H ₂ N	0.08817	0.53422
		COOH	0.00982	0.15667
		C ₈ H ₁₀ N ₄	0.07608	0.03997
		C ₅ H ₂ N	0.01920	0.07236
		R(C ₅ H ₅ S)	0.01715	0.03212
	6	Fe	0.66824	0.06911
		C ₈ H ₁₀ N ₄	0.09489	0.07071
		C ₅ H ₂ N	0.01473	0.08716
		COOH	0.00032	0.00626
		C ₈ H ₁₀ N ₄	0.08301	0.12250
		C ₅ H ₂ N	0.07054	0.45949
		R(C ₅ H ₅ S)	0.07070	0.18719
	9	Fe	0.62688	0.00288
		C ₈ H ₁₀ N ₄	0.15440	0.15556
		C ₅ H ₂ N	0.02090	0.38764
		COOH	0.00044	0.00711
		C ₈ H ₁₀ N ₄	0.16808	0.14028
		C ₅ H ₂ N	0.02453	0.30001
		R(C ₅ H ₅ S)	0.00549	0.00723
NS158	4	Fe	0.69795	0.07436
		C ₈ H ₁₀ N ₄	0.07731	0.07838
		C ₅ H ₂ N	0.07902	0.47009
		COOH	0.00883	0.13761
		C ₈ H ₁₀ N ₄	0.06783	0.04088

	6	C_5H_2N	0.02830	0.12811
		$R(C_6H_3S_2)$	0.04307	0.07286
		Fe	0.64524	0.06901
		$C_8H_{10}N_4$	0.09852	0.08308
		C_5H_2N	0.02251	0.14780
		COOH	0.00107	0.02071
		$C_8H_{10}N_4$	0.08035	0.09624
		C_5H_2N	0.06311	0.38589
		$R(C_6H_3S_2)$	0.09269	0.20074
		Fe	0.62659	0.04316
		$C_8H_{10}N_4$	0.14101	0.14193
		C_5H_2N	0.02316	0.33098
	10	COOH	0.00076	0.00440
		$C_8H_{10}N_4$	0.14061	0.15167
		C_5H_2N	0.03367	0.31349
		$R(C_6H_3S_2)$	0.03466	0.01484
NS271	4	Fe	0.61627	0.06462
		$C_8H_{10}N_4$	0.06402	0.05187
		C_5H_2N	0.05374	0.30340
		COOH	0.00613	0.09173
		$C_8H_{10}N_4$	0.05104	0.04602
		C_5H_2N	0.05003	0.25659
		$R(C_8H_3S_3)$	0.16047	0.18746
		Fe	0.61515	0.07365
	6	$C_8H_{10}N_4$	0.09821	0.10411
		C_5H_2N	0.04544	0.30604
		COOH	0.00371	0.06635
		$C_8H_{10}N_4$	0.08027	0.06989
		C_5H_2N	0.04228	0.23174
		$R(C_8H_3S_3)$	0.11989	0.15318
		Fe	0.33659	0.03583
		$C_8H_{10}N_4$	0.06779	0.02256
	10	C_5H_2N	0.01051	0.02674
		COOH	0.00009	0.00111
		$C_8H_{10}N_4$	0.08318	0.14380
		C_5H_2N	0.07203	0.53154
		$R(C_8H_3S_3)$	0.43215	0.24076
NS252	3	Fe	0.67010	0.03511
		$C_8H_{10}N_4$	0.05431	0.02457
		C_9H_4NS	0.15383	0.56801
		$C_4H_2NO_2$	0.02874	0.32610
		$C_8H_{10}N_4$	0.07899	0.01708
		C_5H_2N	0.00985	0.02229
		$R(C_6H_3S_2)$	0.00671	0.00935
	8	Fe	0.63061	0.06398
		$C_8H_{10}N_4$	0.07948	0.04758
		C_9H_4NS	0.01341	0.04743
		$C_4H_2NO_2$	0.00072	0.01219

13	$C_8H_{10}N_4$	0.05740	0.10304
	C_5H_2N	0.07956	0.48468
	$R(C_6H_3S_2)$	0.14116	0.24344
	Fe	0.21447	0.02980
	$C_8H_{10}N_4$	0.09490	0.08361
	C_9H_4NS	0.38894	0.57001
	$C_4H_2NO_2$	0.17383	0.27085
	$C_8H_{10}N_4$	0.06032	0.01702
	C_5H_2N	0.01374	0.02650
	$R(C_6H_3S_2)$	0.05916	0.00756

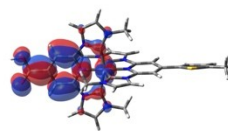
ARM15

HOMO
-5.65 eV



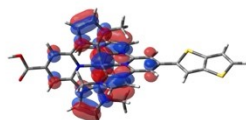
Fe-d: 59.5%

LUMO
-2.95 eV



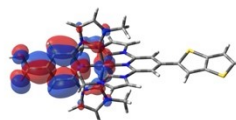
NS158

HOMO
-5.66 eV



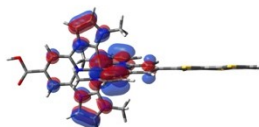
Fe-d: 59.4%

LUMO
-2.97 eV



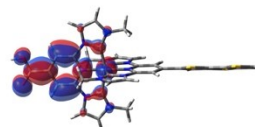
NS271

HOMO
-5.66 eV



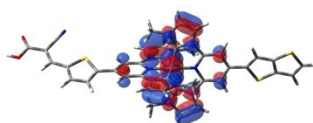
Fe-d: 59.5%

LUMO
-2.97 eV



NS252

HOMO
-5.62 eV



Fe-d: 60.4%

LUMO
-3.48 eV

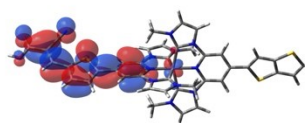


Figure S11: Frontier molecular orbitals (HOMO and LUMO, isovalue 0.02 a.u.) of **ARM15**, **NS158**, **NS271**, and **NS252** computed at the B3LYP*/6-311G(d,p)/C-PCM(ACN) level of theory. The corresponding orbital energies (in eV) and Fe *d*-orbital contributions (%) are reported for each complex.

Characterization of FeNHC-sensitized photoanodes

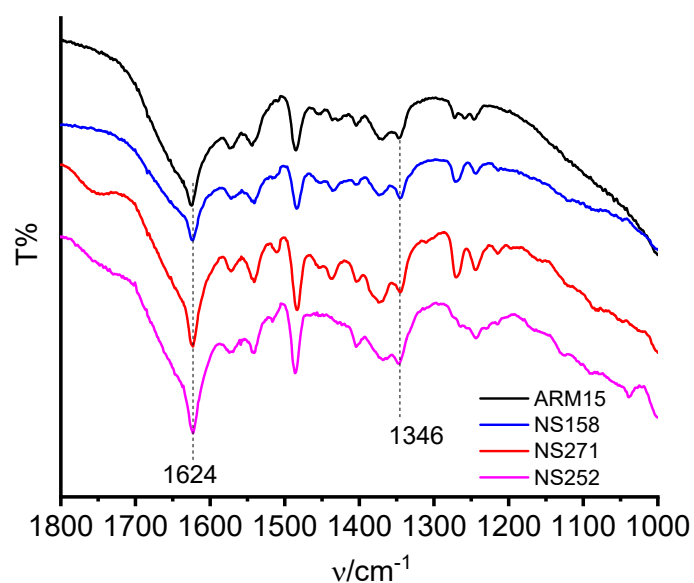


Figure S12: FTIR-ATR spectra of the sensitized TiO_2 photoanodes.

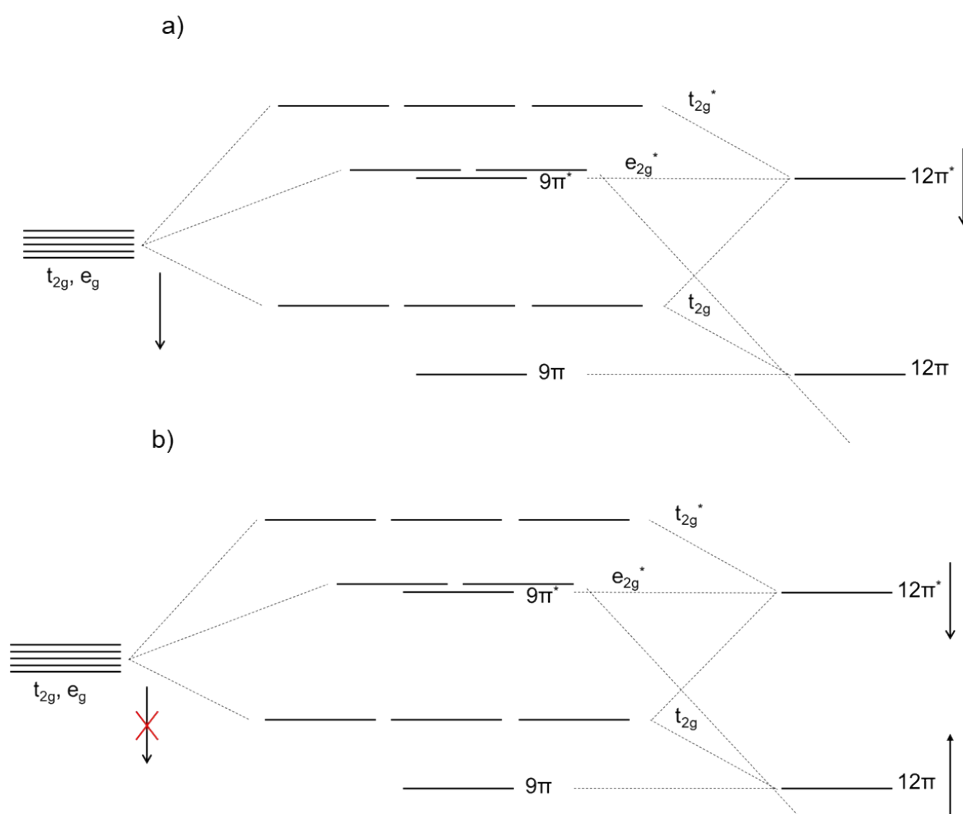


Figure S13: Schematic representation of the molecular orbitals in Fe(II)NHC-based complexes. a) LUMO stabilization leads to a lowering of the t_{2g} orbitals. b) LUMO stabilization is counteracted by the concomitant destabilization of the π -ligand orbitals.

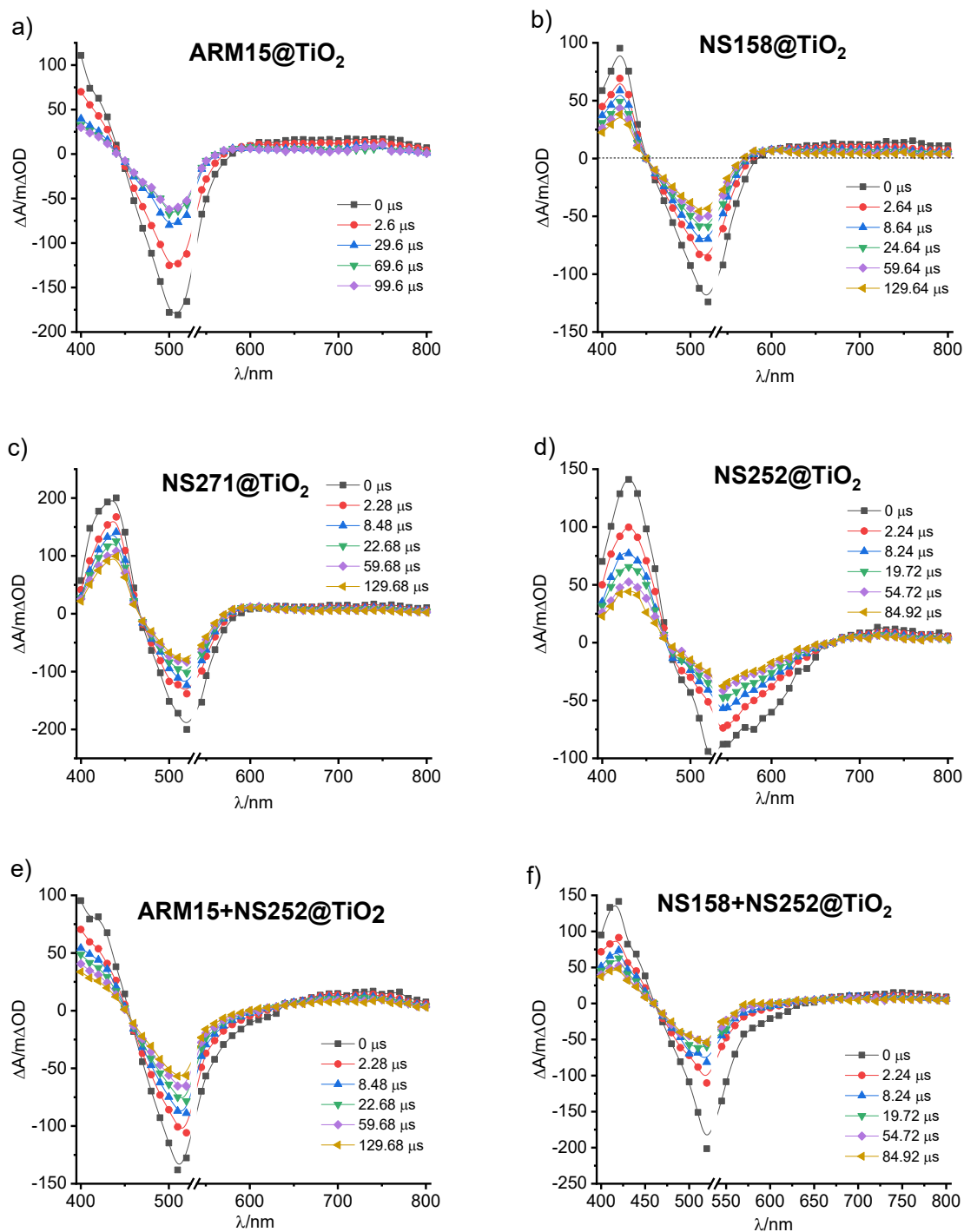


Figure S14: Transient absorption spectra recorded for a) **ARM15**, b) **NS158**, c) **NS271**, d) **NS252**, e) **ARM15+NS252** and f) **NS158+NS252** in contact with 0.1M LiClO₄/ACN solution.

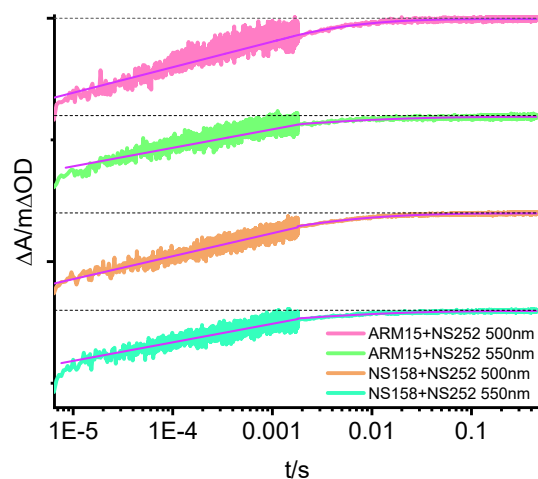


Figure S15: Recombination dynamics collected at 500 and 550 nm for the co-sensitized **ARM15+NS252** and **NS158+NS252** systems in contact with a blank electrolyte (deprived of I^-/I_3^-).

Table S3: Recombination lifetime for the co-sensitized systems extrapolated by using eqs.1a-b and eq.2

Dye	τ_0/s	$\langle\tau\rangle/ms$
ARM15+NS252 – 500 nm	4.49×10^{-5}	1.08
ARM15+NS252 – 550 nm	2.62×10^{-4}	6.29
NS158+NS252 – 500 nm	9.8×10^{-5}	2.35
NS158+NS252 – 550 nm	2.68×10^{-4}	6.43

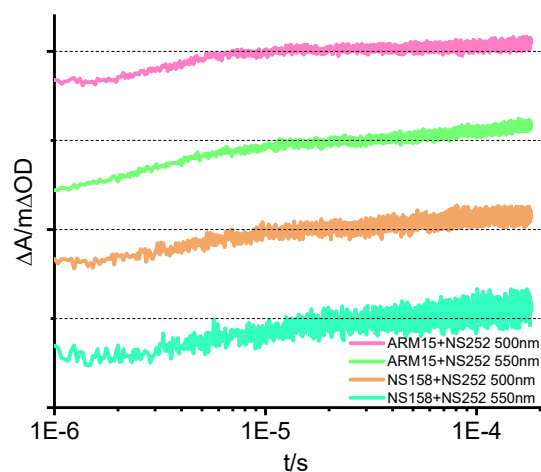


Figure S16: Regeneration dynamics collected at 500 and 550 nm for the co-sensitized **ARM15+NS252** and **NS158+NS252** systems in contact with the reduced form (I^-) of the redox mediator.

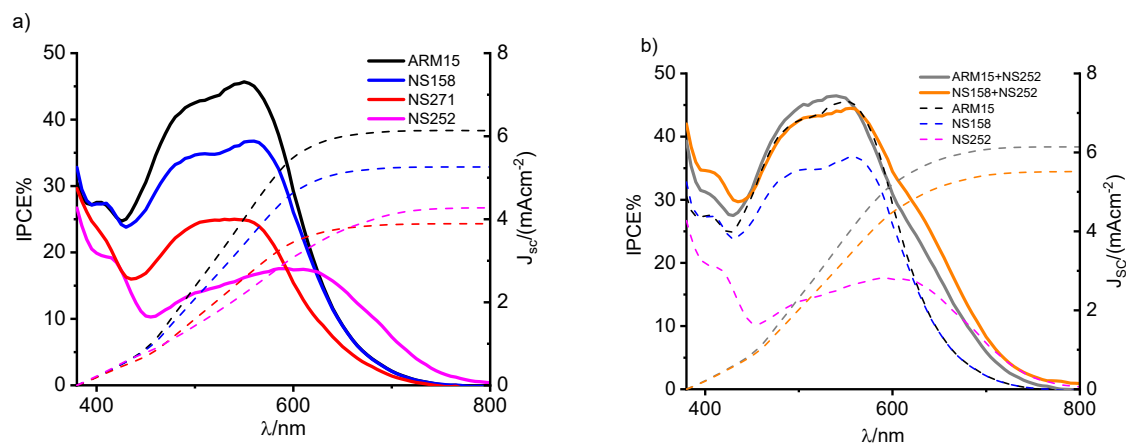


Figure S17: IPCE spectra and integrated photocurrents from 18 μm TiO_2 +scattering layer photoanodes for a) the Fe(II)-NHC family and b) the co-sensitized systems. The IPCE of the individual dyes is also shown.

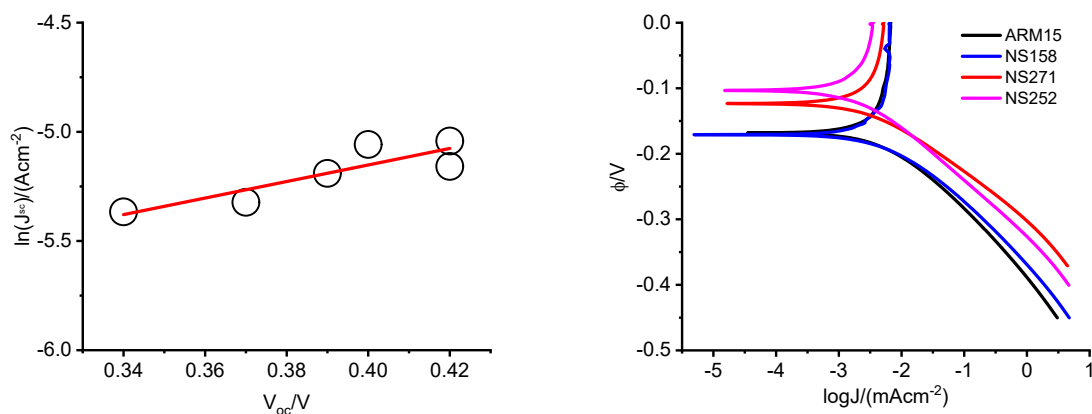


Figure S18: a) $\ln J_{sc}$ vs V_{oc} for the Fe(II)-NHC series. b) Tafel plots of the dark current in Figure 9.

REFERENCES

- [1] A. R. Marri, B. Marekha, T. Penfold, S. Haacke, P. C. Gros, *Inorg. Chem. Front.* **2023**, *10*, 118–126.
- [2] A. Reddy-Marri, E. Marchini, V. D. Cabanes, R. Argazzi, M. Pastore, S. Caramori, P. C. Gros, *Chem. Sci.* **2023**, *14*, 4288–4301.
- [3] A. R. Marri, E. Marchini, V. D. Cabanes, R. Argazzi, M. Pastore, S. Caramori, C. A. Bignozzi, P. C. Gros, *Chem. Eur. J.* **2021**, *27*, 16260–16269.